RSC Advances

PAPER

View Article Online
View Journal | View Issue

Cite this: *RSC Adv.*, 2015, **5**, 60823

New organic dyes with high IPCE values containing two triphenylamine units as co-donors for efficient dye-sensitized solar cells†

Carlos A. Echeverry,[a] Robert Cotta,[b] Edison Castro,[b] Alejandro Ortiz,[a] Luis Echegoyen[b] and Braulio Insuasty*[a]

Here we report the synthetic routes as well as the structural and electronic properties of five new triphenylamine-based organic dyes and their application in dye-sensitized solar cells. In the designed dyes, two triphenylamine groups act as the electron donor units and the electron acceptor is a cyanoacrylic acid, and these units are linked by different π-conjugated spacers including thiophene, dioctylfluorene, ethylcarbazole, and benzo-dithiophene. Density functional theory was employed to study the electron distribution and the intramolecular charge transfer (HOMO–LUMO) of the dyes. Extending the π-conjugation of the dyes broaden and red-shift the bands and improves the light-harvesting ability, however, a device made with triphenylamine maximizer-based dye **TPAM-1** without a π-conjugated spacer exhibited the best photovoltaic performance with a short-circuit photocurrent density (J_{SC}) of 11.37 mA cm^{-2}, an open-circuit voltage (V_{OC}) of 0.836 V, and a fill factor (FF) of 0.603, corresponding to an overall power conversion efficiency of 5.67% under AM 1.5 irradiation (100 mW cm^{-2}).

Received 28th April 2015
Accepted 9th July 2015

DOI: 10.1039/c5ra07720f

www.rsc.org/advances

Introduction

Since the first paper by O'regan and Grätzel,[1] dye-sensitized solar cells (DSSCs) have attracted much attention because they present a highly promising alternative to conventional photovoltaic devices. In a typical DSSC, light is absorbed by the dye molecules anchored to the titanium dioxide (TiO_2) surface, exciting the dye, which then injects electrons from the dye's excited state into the conduction band of the TiO_2, generating an electric current.[2,3] The dye is then restored to its neutral state by electron donation from the electrolyte. So far, DSSCs show photoconversion efficiencies of up to 13.0% which have been observed with polypyridyl ruthenium complexes and zinc porphyrin dyes.[4–6] Interest in metal-free organic sensitizers has grown in recent years because they offer several advantages over other sensitizers: (1) higher molar absorption coefficients due to intramolecular π–π* transitions; (2) easy modification due to relatively short synthetic routes, and (3) tunable electrochemical properties through suitable design.[7]

In these new dyes a covalently linked donor–π-spacer–acceptor (D–π–A)[8–10] structure is used, more specifically, a co-donor system (D–D–π–A).[11–13] The bulkiness of a co-donor system hinders the ability of the electrolyte to reach the semiconductor surface and also inhibits dye aggregation that would otherwise lead to self-quenching and poor electron injection.[14] The role of the co-donor is fulfilled by the bis-triphenylamine (bis-TPA), which is well-known for its easy oxidation and stability. In order to have strong electronic interaction between the TiO_2 and the dye, the choice of the electron acceptor is important; electron acceptors that have been studied are pyridine,[15,16] 3-acetic-rhodanine acid,[17,18] 2-(1,1-dicyanomethylene) rhodanine,[19,20] and cyanoacrylic acid,[21,22] all of which have shown good performance in DSSCs.

In this paper, we have studied the changes in the optical and electrochemical properties upon incorporation of different

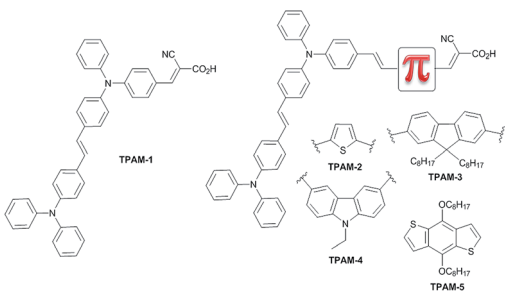

Fig. 1 Molecular structures of **TPAM-(1–5)** dyes.

[a]*Departamento de Química, Facultad de Ciencias Naturales y Exactas, Universidad del Valle, A.A. 25360 Cali, Colombia. E-mail: braulio.insuasty@correounivalle.edu.co; Fax: +57-2-3393248*

[b]*Chemistry and Computer Science, University of Texas at El Paso, 79968-0519 El Paso, Texas, United States. E-mail: echegoyen@utep.edu*

† Electronic supplementary information (ESI) available. See DOI: 10.1039/c5ra07720f

π-conjugated spacers into the bis-TPA skeleton, and their further application as sensitizers in DSSCs. The structures of the bis-TPA based dyes, terminated with the cyanoacrylic acid, are shown in Fig. 1 with the different π-conjugated spacers of thiophene, dioctylfluorene, ethylcarbazole, or benzo-dithiophene.

Results and discussion

Synthesis

In this paper we describe a straightforward synthesis of new dyes using a bis-TPA co-donor system modified with different π-conjugated spacers. The co-donor system (**2**) was prepared by a Horner–Wadsworth–Emmons reaction of compound **1** with 4,4′-diformyltriphenylamine followed by purification, giving rise to the desired product in moderate yields (53%). Compounds **5a–d** were also prepared by a Horner–Wadsworth–Emmons reaction of compound **3** with the corresponding spacer followed by purification, yielding the desired products in moderate yields (45–85%) (see ESI†). The target molecules, **TPAM-(1–5)**, were also prepared in moderate yields (41–71%) through Knoevenagel condensation of cyanoacetic acid and **2**, **5a–d** in glacial acetic acid under reflux. The synthetic procedures followed for the preparation of the TPA-based dyes are shown in Scheme 1. The structures of the new compounds were supported by their analytical and spectroscopic data.

Absorption and emission properties

The absorption spectra of **TPAM-1** recorded in different solvents are shown in Fig. 2. Specifically, **TPAM-1** exhibits two bands around 385 and 450 nm, which can be assigned to the presence of the two TPA groups, the prominent red-shifted band appearing in the range of 400–500 nm is assigned to a charge transfer transition between the electron donor and the cyanoacrylic segment.[23]

Fig. 2a shows that there is a blue shift of the second band when the polarity of the solvent increases in the order $CHCl_3$ < AcOEt < THF < EtOH < DMSO, showing only one band in DMSO and EtOH. The blue shift observed for **TPAM-1** in polar solvents could be attributed to the protonation or deprotonation of the dye, probably due to the more efficient solvation of the dye in these solvents. Deprotonation would occur on the carboxylic acid, diminishing the electron-accepting ability of the

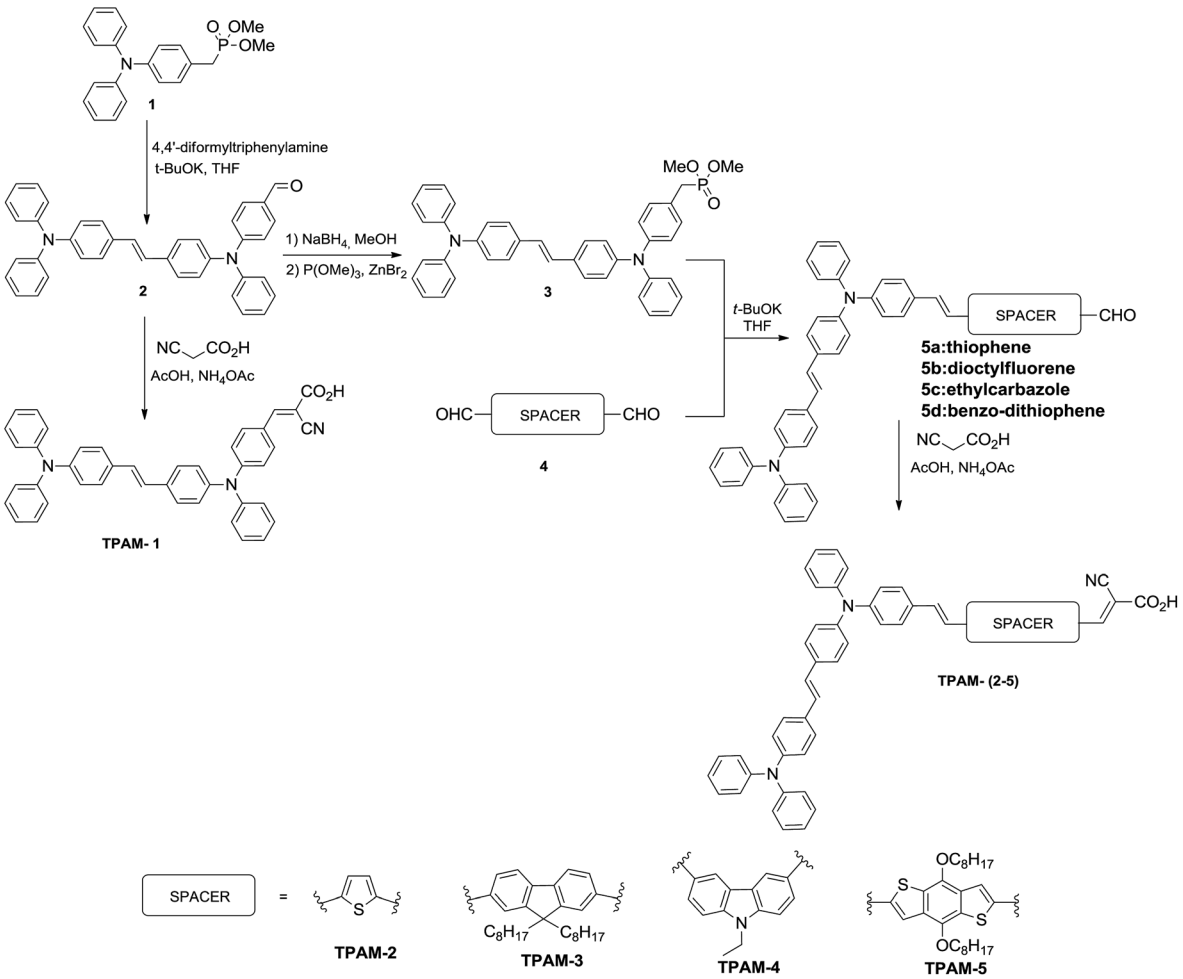

Scheme 1 Synthetic route for the TPAM-(1–5) dyes.

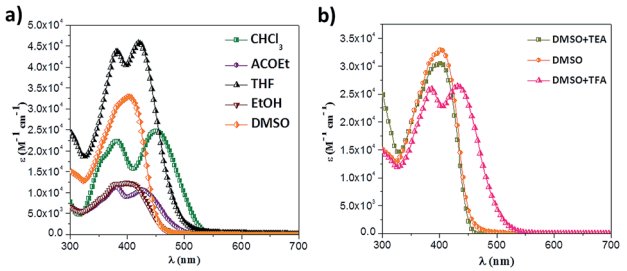

Fig. 2 (a) Absorption spectra of **TPAM-1** in different solvents at a concentration of 1×10^{-5} M; (b) absorption spectra of **TPAM-1** in DMSO before and after the addition of TFA or TEA.

cyanoacrylic acid, which in turn may substantially decrease the donor–acceptor interaction of the dye.[24]

The presence of acid-base equilibria in solution could be confirmed by addition of trifluoroacetic acid (TFA) to the dyes in DMSO. Addition of TFA to the DMSO solution of the dye resulted in a red shift of the charge-transfer band and the appearance of a second band. Since, addition of triethylamine (TEA) to the dye solution did not change the position of the principal band, this leads us to believe that the dye exists in the completely deprotonated form in the ground state (Fig. 2b).

Fig. 3 shows the absorption and emission spectra of the dyes **TPAM-(1–5)** in THF at a concentration of 1×10^{-5} M, with the corresponding data summarized in Table 1. The absorption spectrum for both the thiophene (**TPAM-2**) and benzodithiophene (**TPAM-5**) in solution exhibit similar behavior to that of **TPAM-1**, showing similar bands around 392 and 485 nm but red-shifted by approximately 60 nm. It can be seen that the maximum absorptions of **TPAM-4**, which contains the ethylcarbazole spacer, show a blue shift in comparison with its analogue, **TPAM-3**. This blue shift shown for **TPAM-4** may be attributed to the stabilization of the HOMO orbital and destabilization of the LUMO orbital, which increases the band gap.[25]

The emission spectrum for **TPAM-1** contains a band at 453 nm, corresponding to the maximum emission and a shoulder at 538 nm, corresponding to the second TPA of the bis-TPA. The emission spectra of **TPAM-(2–5)** exhibit a longer bathochromic shift with increasing π-conjugation, especially in the case of **TPAM-3** ($\Delta\lambda_{max}^{em} = 101$ nm) and **TPAM-5** ($\Delta\lambda_{max}^{em} = 97$ nm). The absorption and emission properties of the new compounds both confirm that due to small variations in the π-conjugation

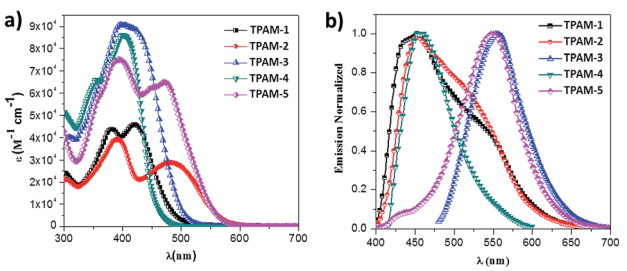

Fig. 3 (a) Molar extinction coefficient plot of **TPAM-(1–5)** in THF; (b) normalized intensity emission in THF.

Table 1 Maximum absorption and emission data of the **TPAM-(1–5)**[a]

Dye	λ_{max}^{abs} (nm) [ε, M^{-1} cm^{-1}]	λ_{max}^{em} (nm)
TPAM-1	421(45 700), 381(43 500)	453
TPAM-2	482(28 700), 395(39 000)	452
TPAM-3	397(90 600)	554
TPAM-4	394(86 000), 355(66 500)	457
TPAM-5	474(66 000), 401(75 000)	550

[a] Absorption and emission spectra of the dyes measured in THF at a concentration of 1×10^{-5} M; ε is the extinction coefficient at the maximum absorption.

length of the system, there are major changes to the photophysical properties of the dye molecules.

Electronic structure quantum calculations

Density functional theory (DFT) calculations were used to understand the electronic structures of **TPAM-(1–5)**. It is interesting to note the *trans* orientation of the bis-TPA and π-conjugated spacers, where the dihedral angle is approximately 180°. Furthermore, the phenyls of the TPAs are not planar but are instead rotated, making it more difficult for the electrolyte to reach the semiconductor surface. The compounds show a quasi-planar π-conjugated spacer-acceptor union; this should facilitate the electronic coupling along the molecule through the spacers. In the case of **TPAM-5**, there is a decrease of the planarity and obviously in the aromaticity of the benzodithiophene spacer, with the dihedral angle between the spacer and bis-TPA at 3.3°, leading to an unfavorable donor–acceptor interaction.

We have also calculated the transition state energies by means a self-consistent field (SCF) method using the CAM-B3LYP functional and the conductor polarized continuum model (CPCM) in THF. The highest occupied molecular orbitals (HOMO−2, HOMO−1 and HOMO) and lowest unoccupied molecular orbitals (LUMO, LUMO+1) of **TPAM-1** are shown in Fig. 4. The HOMO is localized primarily on the co-donor system, whereas the LUMO is mainly localized in the electron-acceptor unit of cyanoacrylic acid with a bridge contribution. The topology of the molecular orbitals of **TPAM-(1–5)** (Fig. 5) is similar to that of **TPAM-1**.

To gain insight into the excited states of the dyes, TDDFT calculations were performed for the lowest six singlet–singlet excitations, and the transitions with oscillator strengths (*f*) are summarized in Table 2. The lowest transition for **TPAM-1** was calculated to be 3.06 eV, corresponding to a charge-transfer excitation from the HOMO−2 to the LUMO and the HOMO−1 to the LUMO with an oscillator strength of 1.4431. The band experimentally found at 3.25 eV (381 nm) appears to correspond to the calculated value of 3.53 eV (351 nm), which is primarily composed of the CT from the HOMO−2 to the LUMO, the HOMO−1 to the LUMO, and the HOMO to the LUMO+1. The excitation characteristics of **TPAM-(2–5)** are similar to the behavior described here for **TPAM-1**; where the lowest transition states are calculated to be 2.60 eV (**TPAM-2**), 2.94 eV

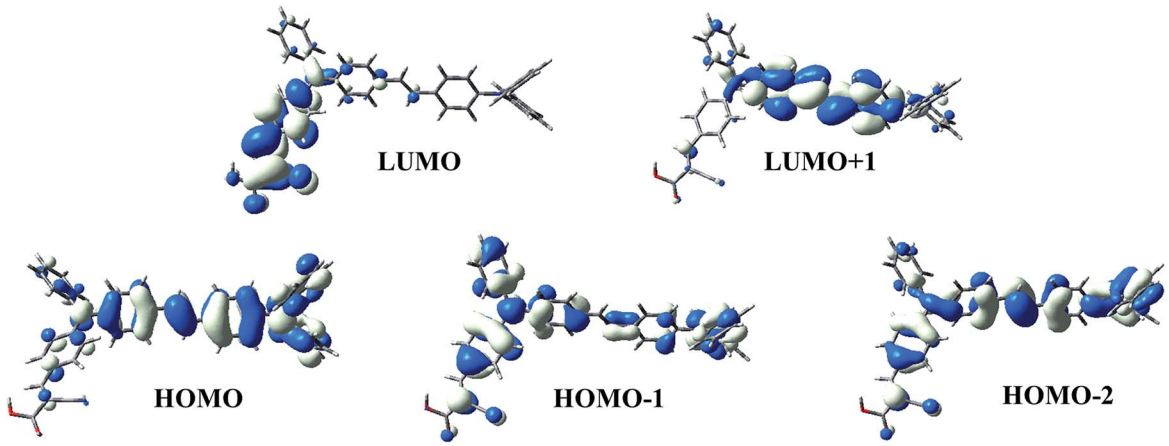

Fig. 4 Frontier molecular orbitals for **TPAM-1**.

(**TPAM-3**), 3.19 eV (**TPAM-4**), and 2.96 eV (**TPAM-5**). A bathochromic shift is observed when the π-conjugation length is increased across the spacer, except for **TPAM-4**, which agrees with the experimentally observed hypsochromic shift.

Electrochemical properties

The oxidation potential *vs.* NHE (E_{ox}) corresponds to the highest occupied molecular orbital (HOMO) and its energy was calculated using eqn (1).[26] The excited state energy (E_{LUMO}) is important in determining the feasibility of an electron transferring from the dye into the conduction band of the TiO_2. An approximation of E_{LUMO} can be calculated from the energy of the ground state oxidation (E_{HOMO}) and the zero–zero excitation energy (E_{0-0}) as follows $E_{HOMO} + E_{0-0}$.[27]

$$E_{HOMO} = -(E_{ox} + 4.75)\ \text{eV} \quad (1)$$

The E_{ox} of the as-synthesized dyes were obtained from the cyclic voltammogram for each dye and the results are summarized in Table 3. The onset oxidative potentials (E_{ox}) of the dyes yield HOMO level energies in the range of −5.58 to −5.47 eV, lower than that of the electrolyte redox couple (4.90 eV),[27] ensuring that there is efficient dye regeneration. The introduction of the π-conjugation promotes a decrease in the oxidation potentials, most likely due to the stabilization of the oxidized or reduced species across the entire molecule. Most significant is the addition of the benzo-dithiophene unit in **TPAM-5** that leads to a decrease in the E_{ox} of 0.112 V when compared with the value for **TPAM-1**, thus lowering the driving force resulting from the reduction of the oxidized dye by the electrolyte. The energy gap (E_{gap}) between the LUMO level of the dyes and the conduction band edge of the TiO_2 (−3.90 eV) should be at least 0.2 eV for efficient electron injection. The E_{gap} ranges from

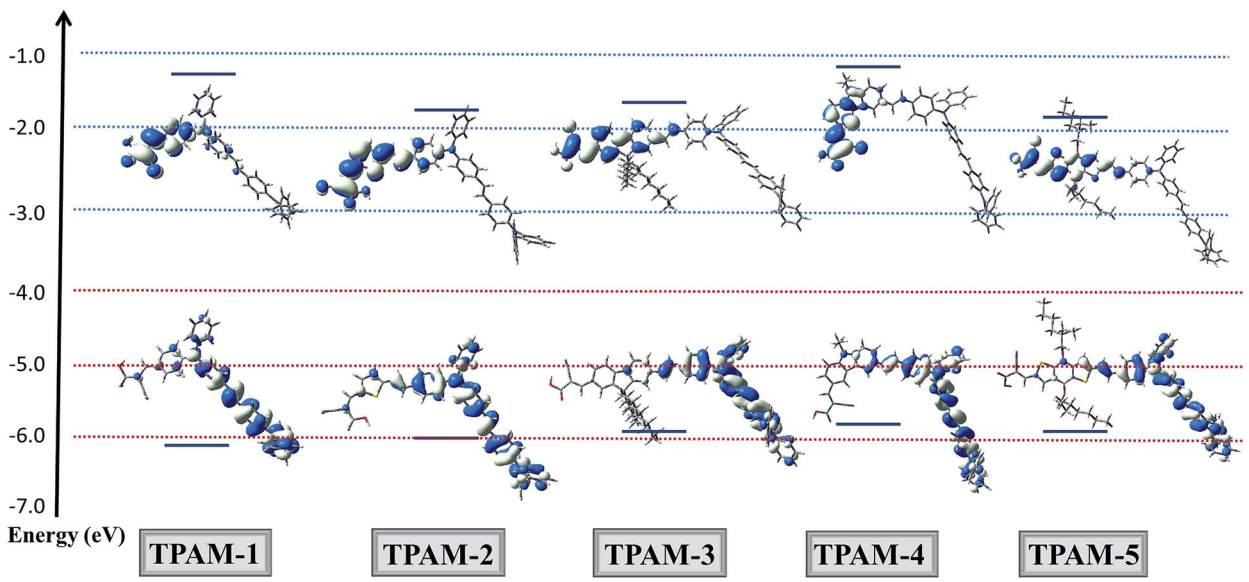

Fig. 5 Energies and electronic distribution of the frontier molecular orbitals of the dyes **TPAM-(1–5)** computed in THF using TDDFT/CAM-B3LYP/6-31G(d, p).

Table 2 Calculated TD-DFT excitation energies (E), oscillator strengths (f), and character (CT = charge transfer)[a]

Dye	E^a/eV (nm)	Composition	Character	E/eV (nm)	f
TPAM-1	2.94(421)	H−2 → L(0.12)	CT	3.06(405)	1.4431
		H−1 → L(0.46)			
	3.25(381)	H−2 → L(0.13)	CT	3.53(351)	1.3163
		H−1 → L(0.28)	CT		
		H → L + 1(0.60)	π–π*		
TPAM-2	2.57(482)	H−1 → L(0.42)	CT	2.60(476)	1.8212
		H → L(0.47)	CT		
	3.14(395)	H−1 → L(0.18)	CT	3.39(366)	1.5291
		H → L + 1(0.56)	π–π*		
TPAM-3	3.12(397)	H−1 → L(0.33)	CT	2.94(422)	2.6710
		H → L(0.40)			
		H → L + 1(0.49)	π–π*	3.37(368)	1.1985
		H → L + 2(0.33)			
TPAM-4	3.15(394)	H−2 → L(0.27)	CT	3.19(389)	1.4118
		H → L(0.30)	CT		
	3.49(355)	H−1 → L(0.21)	CT	3.39(366)	1.9393
		H → L + 1(0.47)	π–π*		
		H → L + 2(0.18)	π–π*		
TPAM-5	2.61(474)	H−1 → L(0.64)	CT	2.96(419)	0.3988
		H−3 → L(0.27)	π–π*	3.68(337)	1.6166
		H−2 → L(0.34)	CT		
	3.09(401)	H → L + 1(0.52)	π–π*	4.04(307)	1.1606

[a] E is the experimental value of energy calculated from the absorption spectra: $E = 1240/\lambda$ (Table 1).

0.82 to 1.27 eV for the bis-TPA dyes which are more than sufficient for electron injection into the conduction band of the TiO_2 (Fig. 6).

Solar cells performance

Fig. 7a shows the incident photo-conversion efficiency (IPCE) for DSSCs composed of the dyes **TPAM-(1–5)** and the standard **N719**. It can be seen that the photocurrent response of the **TPAM-1** DSSC exceeds 90% in the range between 375 and 500 nm, which is higher than the response of the **N719** DSSC (76% in the range of 516–531 nm, similar to the value reported in the literature).[2]

The broadening of the IPCE spectra is desired for a larger photocurrent which explains the higher efficiency observed for **N719**. Generally, an increase of the π-conjugation in the dyes

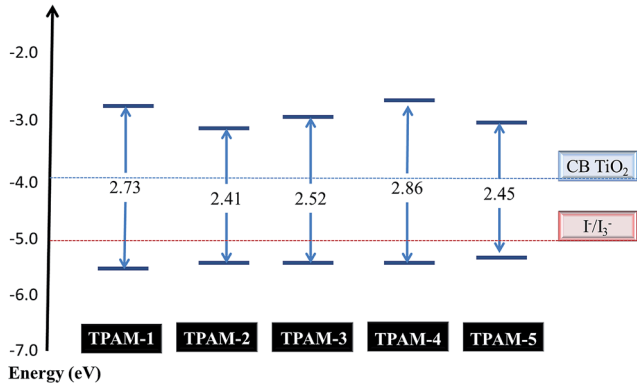

Fig. 6 Comparison of the E_{HOMO} and E_{LUMO} levels of the dyes **TPAM-(1–5)** with the energy of the conduction band of the TiO_2 and redox couple.

extends the spectral absorption towards longer wavelengths, leading to a broadening of the spectral region, which is important for light harvesting. In the case of **TPAM-2**, the presence of the spacer based on thiophene enhanced the breadth of the IPCE curve with a maximum value of 81% at 427 nm, yielding the highest photocurrent response comparable to that of the device based on **N719**. **TPAM-3** also showed a high IPCE of 91% at 450 nm and effective light harvesting up to about 550 nm, however, the presence of the dioctylfluorene did not lead to an increase in the breadth of the IPCE curve, yielding a lower photocurrent response when compared to **TPAM-2**. Fig. 7b shows the corresponding photocurrent density–voltage (J–V) curves of the fabricated DSSCs under AM 1.5 solar irradiation (100 mW cm^{-2}). The photovoltaic data are summarized in Table 4, and the photoconversion efficiencies (PCEs) from lowest to highest were **TPAM-4** < **TPAM-5** < **TPAM-2** < **TPAM-3** < **TPAM-1**. The DSSC based on **TPAM-1** showed the best overall PCE at 5.67% with an open circuit voltage of 0.836 V, a short circuit photocurrent density of 11.37 mA cm^{-2}, and a fill factor of 0.603.

The dyes **TPAM-1**, **TPAM-2** and **TPAM-3** showed the highest J_{sc} values, indicating better electron injection which is also observed in Fig. 7b. **TPAM-2** showed a J_{sc} of 12.20 mA cm^{-2}, which can be attributed to the wider absorption spectrum observed and its higher IPCE values in a broad wavelength range.

Table 3 Electrochemical data of the as-synthetized dyes

Dye	λ_{int} (nm)	$E_{0-0}{}^a$ (eV)	$E_{ox}{}^b$ (V)	$E_{HOMO}{}^c$ (eV)	$E_{LUMO}{}^d$ (eV)	$E_{gap}{}^e$ (eV)
TPAM-1	455	2.73	0.83	−5.58	−2.85	1.05
TPAM-2	515	2.41	0.74	−5.49	−3.08	0.82
TPAM-3	492	2.52	0.74	−5.49	−2.97	0.93
TPAM-4	433	2.86	0.74	−5.49	−2.63	1.27
TPAM-5	505	2.45	0.72	−5.47	−3.02	0.88

[a] E_{0-0} values were calculated from the intercept of the normalized adsorption and the emission spectra (λ_{int}): $E_{0-0} = 1240/\lambda_{int}$. [b] Potentials measured *vs.* the (Fc/Fc^+) couple were converted to normal hydrogen electrode (NHE) by addition of +0.63 V. [c] Calculated with the formula $E_{HOMO} = -(E_{ox} + 4.75)$ eV. [d] Calculated with the formula $E_{LUMO} = (E_{HOMO} + E_{0-0})$ eV. [e] E_{gap} is the energy gap between the E_{LUMO} of dye and the conduction band level of TiO_2 (−3.90 eV).[27]

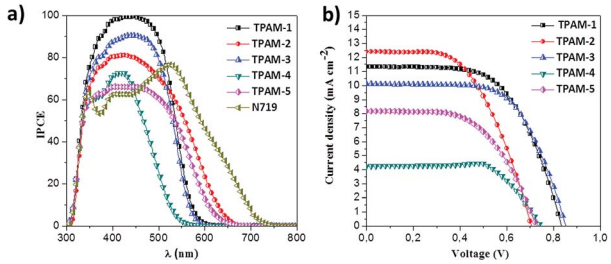

Fig. 7 (a) IPCE spectra for DSSCs based on the as-synthetized dyes; (b) current density–voltage characteristics for the DSSCs based on **TPAM-(1–5)**.

Table 4 Photovoltaic performance of DSSCs sensitized with **TPAM-(1–5)** with the standard **N719** for comparison

Dye	J_{sc} (mA cm^{-2})	V_{oc} (V)	FF	PCE (%)
TPAM-1	11.37	0.836	0.603	5.67
TPAM-2	12.20	0.709	0.556	4.83
TPAM-3	10.15	0.851	0.635	5.41
TPAM-4	4.24	0.737	0.734	2.26
TPAM-5	8.11	0.730	0.584	3.39
N719	15.04	0.804	0.534	6.31

It can also be seen that the introduction of the thiophene in **TPAM-2** leads to a lower V_{oc} and FF, which results in an overall decrease in efficiency. This behaviour have already been shown by similar systems, because the introduction of thiophene leads generally a poor regeneration of the oxidized dyes, which have been confirmed in a previous studies done for us, where the introduction of thiophene spacer also leads to a lower V_{oc} and FF because of a poor regeneration of the oxidized dyes.

The lower photocurrent response of **TPAM-4** can be attributed to the compression of the absorption spectrum due to the higher energy band-gap and the isolation of the HOMO–LUMO levels that lead to unfavorable electron transport, overall displaying poor donor–acceptor behavior. All above mentioned points were corroborated by mean of electronic calculations for the dye, which also showed a isolating of the HOMO and LUMO levels that led to a bad communication between the co-donor system and the acceptor based in cyanoacrylic acid, which can be observed in the lowest overall efficiency for **TPAM-4** compared with the other dyes.

In the case of **TPAM-5**, it can be seen that the introduction of the benzo-dithiophene, like the thiophene, leads to a lower V_{oc} and FF. Furthermore, although there is a broad absorption spectrum leading to a J_{sc} of 8.11 mA cm^{-2}, electron transport is limited, due to the decrease in the planarity of the molecule. The effect of loss of the planarity can be seen in the IPCE values, which showed a decrease in the values for **TPAM-5**. The decrease observed in IPCE values is according to the systems based in thiophene and is greater when there are an increase of the number of thiophenes in the π-conjugation.[28] Cyclic voltammetry showed that the onset oxidative potentials (E_{ox} *vs.* NHE) ranging from 0.72 to 0.83 V yield HOMO levels more positive than the oxidation potential for I^-/I_3^- (0.35 V *vs.* NHE),[29] therefore the energy levels for **TPAM-(1–5)** fulfilled the requirement for effective electron injection and dye regeneration.

Conclusions

We have prepared and fully characterized five new co-donor based dyes for DSSC applications. Using DFT calculations and frontier orbital analysis, it is evident that the HOMO is typically localized on the electron-donor moiety and the LUMO is localized on the electron-acceptor unit, where the different π-bridges influence the push–pull effect of the dyes. The increased π-conjugation of the dyes tends to broaden and red-shift the absorption bands to improve the light-harvesting effect, however, a device made with **TPAM-1** (no π-conjugated spacer) exhibited the best photovoltaic results with a short-circuit photocurrent density (J_{sc}) of 11.37 mA cm^{-2}, an open-circuit voltage (V_{oc}) of 0.836 V, and a fill factor (FF) of 0.603, corresponding to an overall power conversion efficiency of 5.67%. This is most likely due to the effectiveness of the dye to inject electrons into the conduction band of the TiO_2, as exhibited in the calculations.

Experimental section

Materials and reagents

Solvents were dried according to standard procedures and reagents were used as purchased unless otherwise noted. All air-sensitive reactions were carried out under argon. Flash chromatography was performed using silica gel (Merck, Kieselgel 60, 230–240 mesh or Scharlau 60, 230–240 mesh). Analytical thin layer chromatography (TLC) was performed on aluminum coated with Merck Kieselgel 60 F254. Melting points were determined on a Sanyo Gallenkamp melting point apparatus. NMR spectra were recorded on a Bruker Avance 400 (^{1}H: 400 MHz; ^{13}C: 100 MHz) spectrometer at 298 K using deuterated solvents as internal standards. Coupling constants (J) are reported in Hz and chemical shifts (δ) in ppm. Multiplicities are denoted as follows: s = singlet, d = doublet, t = triplet, q = quartet, m = multiplet, br = broad. FT-IR spectra were recorded on a Shimadzu FT-IR 8400 spectrometer. UV-Vis spectra were recorded on a Shimadzu 1700 spectrometer. Mass spectra were scanned on a Shimadzu MS-QP 2010 spectrometer operating at 70 eV and Matrix Assisted Laser Desorption Ionization Time-Of-Flight (MALDI-TOF) were recorded on a HP1100MSD spectrometer and a Bruker REFLEX spectrometer.

Electrochemical measurements

The electrochemical properties of the dyes were studied with an AutolabPGStat 30 at a scan rate of 100 mV s^{-1}, using a glassy carbon working electrode, a platinum wire counter electrode, and a silver wire pseudo-reference electrode. Tetra-*n*-butylammonium hexafluorophosphate ($TBAPF_6$) (0.1 M) was used as the supporting electrolyte in dry dichloromethane (DCM) and samples were purged with argon prior to the measurements. All

potentials are reported *versus* a ferrocene/ferrocenium (Fc/Fc^+) internal reference.

Computation methods

The geometric and electronic properties of the new dyes were calculated with Gaussian 09. The geometry was optimized for each dye by means of the B3LYP and a 6-31G(d, p) basis set and the excitation transitions were calculated using time dependent density functional theory (TDDFT) calculations with CAM-B3LYP/6-31G(d, p).[30]

Cell fabrication and testing

Fluorine-doped tin oxide (FTO) coated glass (TEC7) was cleaned in detergent and ethanol before being treated with a 40 mM aqueous solution of titanium(IV) tetrachloride ($TiCl_4$) for 30 min at 70 °C. Devices were structured with three layers that were doctor-bladed using transparent, semitransparent, and opaque TiO_2 pastes. After the final layer was bladed, films were sintered at 450 °C for 30 minutes. Prior to dye adsorption, the devices were again treated with 40 mM $TiCl_4$, and annealed at 500 °C for 30 minutes. Once cooled, the corresponding dye was adsorbed onto the photoanode surface by soaking the electrode in a dye solution (either dry DCM, THF, and/or a mixture of THF : EtOH 10 : 1) at a concentration of 0.3 mM at room temperature for 24 h. Pt counter electrodes were produced by spin coating a 2 mg mL^{-1} solution of chloroplatinic acid (H_2PtCl_6) in ethanol onto cleaned FTO and heated at 400 °C for 15 min. Solar cells were made by sealing the electrolyte solution (0.6 M 1,2-dimethyl-3-propylimidazolium iodide (DMPII), 0.1 M guanidinium thiocyanate, 0.03 M I_2, 0.5 M 4-*tert*-butylpyridine in dry acetonitrile) between the dye coated photoanode (approx. 0.25 cm^2) and the Pt counter electrode. Photovoltaic measurements were then made using a Photo Emission Tech Solar Simulator SS100 at AM 1.5 conditions.

Synthetic procedure for TPAM-(1–5) dyes

As shown in Scheme 1, the corresponding aldehyde (**2**, **5a–d**) (50 mg), 3-cyanoacetic acid (4 eq.), ammonium acetate (100 mg) and glacial acetic acid (15 mL) were stirred and heated at 120 °C for 10 h. The acetic acid was evaporated and the solid was washed with water and filtered. The solid obtained was purified further by recrystallization from ethanol and column chromatography (**TPAM-3** and **TPAM-5**).

TPAM-1. Red solid, (40 mg, 71%), mp > 350 °C. ^{1}H-NMR (DMSO-d_6, 400 MHz) δ: 7.97 (s, 1H), 7.79 (d, J = 8 Hz, 2H), 7.49 (d, J = 8 Hz, 2H), 7.40 (d, J = 8 Hz, 2H), 7.34–7.31 (m, 2H), 7.23–7.20 (m, 4H), 7.15–7.09 (m, 3H), 7.03 (br, 4H), 6.98–6.93 (m, 6H), 6.85 (br, 4H) ppm; ^{13}C-NMR (DMSO-d_6, 100 MHz) δ: 169.7, 161.4, 146.9, 146.7, 145.0, 132.4, 131.4, 130.0, 129.6, 127.7, 127.6, 126.2, 126.0, 125.9, 124.1, 123.3, 123.0, 119.3, 99.5, 63.1 ppm; FTIR (KBr) ν: 3390 (O–H), 2218 (CN), 1718 (C=O), 1506, 1487 cm^{-1}; MS (MALDI-TOF): calcd for $C_{42}H_{31}N_3O_2$ 609.241; found 609.237 [M^+].

TPAM-2. Black solid, (32 mg, 48%), mp > 350 °C. ^{1}H-NMR (DMSO-d_6, 400 MHz) δ: 8.45 (s, 1H), 7.94 (d, J = 4 Hz, 1H), 7.59 (d, J = 8 Hz, 2H), 7.54–7.47 (m, 4H), 7.43–7.41 (m, 2H), 7.37–7.31 (m, 6H), 7.24 (d, J = 16 Hz, 1H), 7.16–7.10 (m, 6H), 7.07–7.03 (m, 7H), 6.99–6.95 (m, 4H) ppm; ^{13}C-NMR (DMSO-d_6, 100 MHz) δ: 164.3, 153.2, 148.1, 147.5, 147.0, 146.9, 146.2, 134.0, 133.1, 132.8, 132.0, 130.3, 130.1, 128.9, 128.0, 127.9, 127.4, 126.7, 125.4, 125.0, 124.8, 124.6, 123.7, 123.6, 122.8, 122.2, 117.2, 100.0, 97.9, 79.3, 55.6 ppm; FTIR (KBr) ν: 3398 (O–H), 2230 (CN), 1709 (C=O), 1431 cm^{-1}; MS (MALDI-TOF): calcd for $C_{48}H_{35}N_3O_2S$ 717.245; found 717.235 [M^+].

TPAM-3. Red solid, (39 mg, 41%), mp > 350 °C. ^{1}H-NMR (DMSO-d_6, 400 MHz) δ: 8.25 (s, 1H), 8.09 (s, 1H), 8.00–7.94 (m, 2H), 7.88 (d, J = 8 Hz, 1H), 7.72 (s, 1H), 7.59 (d, J = 8 Hz, 1H), 7.56 (d, J = 8 Hz, 2H), 7.50 (t, J = 8 Hz, 4H), 7.36 (d, J = 8 Hz, 2H), 7.34–7.30 (m, 5H), 7.23 (d, J = 16 Hz, 1H), 7.12–7.00 (m, 15H), 6.95 (d, J = 8 Hz, 2H), 2.04–2.00 (m, 4H), 1.23–1.00 (m, 21H), 0.75 (t, J = 8 Hz, 6H), 0.54 (br, 4H) ppm; ^{13}C-NMR (DMSO-d_6, 100 MHz) δ: 152.8, 151.8, 147.6, 147.3, 147.2, 146.7, 139.1, 138.4, 136.4, 132.4, 131.8, 131.7, 129.4, 129.3, 128.6, 127.5, 127.2, 127.2, 126.9, 126.5, 125.4, 124.8, 124.5, 124.2, 123.7, 123.4, 123.0, 120.8, 120.2, 58.6, 55.3, 31.8, 30.0, 29.2, 23.9, 22.6, 14.1 ppm; FTIR (KBr) ν: 3359 (O–H), 2924, 2854, 2219, 1586 (C=O), 1273 cm^{-1}; MS (MALDI-TOF): calcd for $C_{73}H_{73}N_3O_2$ 1023.570; found 1023.603 [M^+].

TPAM-4. Orange solid, (60 mg, 56%), mp > 350 °C. ^{1}H-NMR (DMSO-d_6, 400 MHz) δ: 13.69 (s, 1H), 8.88 (s, 1H), 8.45 (s, 1H), 8.34 (s, 1H), 8.29 (d, J = 8 Hz, 1H), 7.85–7.83 (m, 2H), 7.73 (d, J = 8 Hz, 1H), 7.58 (d, J = 8 Hz, 2H), 7.50 (t, J = 8 Hz, 4H), 7.39–7.30 (m, 7H), 7.26 (d, J = 16 Hz, 1H), 7.09–7.03 (m, 15H), 6.96 (d, J = 8 Hz, 2H), 4.53 (q, J = 4 Hz, 2H), 1.36 (t, J = 4 Hz, 3H) ppm; ^{13}C-NMR (DMSO-d_6, 100 MHz) δ: 164.6, 147.5, 147.3, 146.9, 146.7, 146.5, 143.0, 140.3, 132.6, 132.4, 132.2, 130.6, 130.1, 130.0, 128.1, 127.9, 127.0, 126.8, 126.5, 125.9, 125.8, 124.8, 124.5, 124.1, 124.0, 123.9, 123.7, 123.6, 123.2, 123.1, 123.0, 119.1, 110.9, 110.8, 55.4, 31.2, 14.3 ppm; FTIR (KBr) ν: 3414 (O–H), 2923, 2220 (CN), 1606 (C=O), 1190 cm^{-1}; MS (MALDI-TOF): calcd for $C_{58}H_{44}N_4O_2$ 828.346; found 828.389 [M^+].

TPAM-5. Red solid, (75 mg, 54%), mp > 350 °C. ^{1}H-NMR (DMSO-d_6, 400 MHz) δ: 8.40 (s, 1H), 8.27 (s, 1H), 7.57–7.48 (m, 8H), 7.37 (d, J = 8 Hz, 2H), 7.33 (d, J = 8 Hz, 2H), 7.31 (d, J = 8 Hz, 2H), 7.14 (d, J = 8 Hz, 2H), 7.11–7.01 (m, 12H), 6.99 (d, J = 8 Hz, 2H), 6.96 (d, J = 8 Hz, 2H), 4.33–4.24 (m, 4H), 1.83–1.77 (m, 4H), 1.55–1.48 (m, 4H), 1.33–1.23 (m, 16H), 0.87–0.84 (m, 6H) ppm; ^{13}C-NMR (DMSO-d_6, 100 MHz). δ: 147.7, 147.5, 147.0, 146.3, 145.3, 143.4, 132.9, 132.1, 131.7, 130.6, 130.2, 130.0, 129.9, 128.7, 128.5, 128.0, 127.9, 127.2, 126.7, 125.3, 124.6, 124.5, 124.4, 123.7, 123.1, 55.4, 31.7, 30.4, 29.2, 29.1, 26.0, 25.8, 22.6, 14.4 ppm; FTIR (KBr) ν: 3350 (O–H), 2922, 2213 (CN), 1589 (C=O), 1273 cm^{-1}; MS (MALDI-TOF): calcd for $C_{70}H_{69}N_3O_4S_2$ 1079.472; found 1079.566 [M^+].

Acknowledgements

The authors gratefully acknowledge financial support from COLCIENCIAS, Universidad del Valle, Robert A. Welch foundation for an endowed chair (Grant # AH-0033), U.S. Air force grants (AFOSR-FA9550-12-1-0053 and AFOSR-AF9559-12-1-0468), and the U.S. NSF (Grant DMR-1205302).

Notes and references

1 B. O'regan and M. Grätzel, *Nature*, 1991, **353**, 737–740.
2 M. Grätzel, *Inorg. Chem.*, 2005, **44**, 6841–6851.
3 A. Hagfeldt, G. Boschloo, L. Sun, L. Kloo and H. Pettersson, *Chem. Rev.*, 2010, **110**, 6595–6663.
4 A. Yella, H.-W. Lee, H. N. Tsao, C. Yi, A. K. Chandiran, M. K. Nazeeruddin, E. W.-G. Diau, C.-Y. Yeh, S. M. Zakeeruddin and M. Grätzel, *Science*, 2011, **334**, 629–634.
5 T. Bessho, S. M. Zakeeruddin, C. Y. Yeh, E. W. G. Diau and M. Grätzel, *Angew. Chem., Int. Ed.*, 2010, **49**, 6646–6649.
6 S. Mathew, A. Yella, P. Gao, R. Humphry-Baker, B. F. Curchod, N. Ashari-Astani, I. Tavernelli, U. Rothlisberger, M. K. Nazeeruddin and M. Grätzel, *Nat. Chem.*, 2014, **6**, 242–247.
7 A. Mishra, M. K. Fischer and P. Bäuerle, *Angew. Chem., Int. Ed.*, 2009, **48**, 2474–2499.
8 S. Wenger, P.-A. Bouit, Q. Chen, J. Teuscher, D. D. Censo, R. Humphry-Baker, J.-E. Moser, J. L. Delgado, N. Martín and S. M. Zakeeruddin, *J. Am. Chem. Soc.*, 2010, **132**, 5164–5169.
9 D. G. Patel, N. M. Bastianon, P. Tongwa, J. M. Leger, T. V. Timofeeva and G. P. Bartholomew, *J. Mater. Chem.*, 2011, **21**, 4242–4250.
10 W. Zeng, Y. Cao, Y. Bai, Y. Wang, Y. Shi, M. Zhang, F. Wang, C. Pan and P. Wang, *Chem. Mater.*, 2010, **22**, 1915–1925.
11 T. Sudyoadsuk, S. Pansay, S. Morada, R. Rattanawan, S. Namuangruk, T. Kaewin, S. Jungsuttiwong and V. Promarak, *Eur. J. Org. Chem.*, 2013, **2013**, 5051–5063.
12 Y. Liang, B. Peng and J. Chen, *J. Phys. Chem. C*, 2010, **114**, 10992–10998.
13 S. Wang, H. Wang, J. Guo, H. Tang and J. Zhao, *Dyes Pigm.*, 2014, **109**, 96–104.
14 Z. Ning and H. Tian, *Chem. Commun.*, 2009, 5483–5495.
15 J. Mao, D. Wang, S. H. Liu, Y. Hang, Y. Xu, Q. Zhang, W. Wu, P. T. Chou and J. Hua, *Asian J. Org. Chem.*, 2014, **3**, 153–160.
16 J. Lu, X. Xu, Z. Li, K. Cao, J. Cui, Y. Zhang, Y. Shen, Y. Li, J. Zhu and S. Dai, *Chem.–Asian J.*, 2013, **8**, 956–962.
17 C.-H. Yang, H.-L. Chen, Y.-Y. Chuang, C.-G. Wu, C.-P. Chen, S.-H. Liao and T.-L. Wang, *J. Power Sources*, 2009, **188**, 627–634.
18 C. A. Echeverry, M. A. Herranz, A. Ortiz, B. Insuasty and N. Martin, *New J. Chem.*, 2014, **38**, 5801–5807.
19 J. Mao, N. He, Z. Ning, Q. Zhang, F. Guo, L. Chen, W. Wu, J. Hua and H. Tian, *Angew. Chem., Int. Ed.*, 2012, **124**, 10011–10014.
20 C. A. Echeverry, A. Insuasty, M. Á. Herranz, A. Ortíz, R. Cotta, V. Dhas, L. Echegoyen, B. Insuasty and N. Martín, *Dyes Pigm.*, 2014, **107**, 9–14.
21 M. Marszalek, S. Nagane, A. Ichake, R. Humphry-Baker, V. Paul, S. M. Zakeeruddin and M. Grätzel, *J. Mater. Chem.*, 2012, **22**, 889–894.
22 C. Sakong, H. J. Kim, S. H. Kim, J. W. Namgoong, J. H. Park, J.-H. Ryu, B. Kim, M. J. Ko and J. P. Kim, *New J. Chem.*, 2012, **36**, 2025–2032.
23 H. Tian, X. Yang, J. Pan, R. Chen, M. Liu, Q. Zhang, A. Hagfeldt and L. Sun, *Adv. Funct. Mater.*, 2008, **18**, 3461–3468.
24 A. Baheti, P. Singh, C.-P. Lee, K. J. Thomas and K.-C. Ho, *J. Org. Chem.*, 2011, **76**, 4910–4920.
25 A. Baheti, P. Tyagi, K. J. Thomas, Y.-C. Hsu and J. T. s. Lin, *J. Phys. Chem. C*, 2009, **113**, 8541–8547.
26 C. M. Cardona, W. Li, A. E. Kaifer, D. Stockdale and G. C. Bazan, *Adv. Mater.*, 2011, **23**, 2367–2371.
27 L. Yu, K. Fan, T. Duan, X. Chen, R. Li and T. Peng, *ACS Sustainable Chem. Eng.*, 2014, **2**, 718–725.
28 P. Qin, X. Yang, R. Chen, L. Sun, T. Marinado, T. Edvinsson, G. Boschloo and A. Hagfeldt, *J. Phys. Chem. C*, 2007, **111**, 1853–1860.
29 G. Boschloo and A. Hagfeldt, *Acc. Chem. Res.*, 2009, **42**, 1819–1826.
30 N. Martsinovich and A. Troisi, *Energy Environ. Sci.*, 2011, **4**, 4473–4495.